Trans Indian Inst Met (2017) 70(7):1795–1804
DOI 10.1007/s12666-016-0978-5

TECHNICAL PAPER

An Approach for Estimation of Cathode Voltage Drop in an Aluminum Reduction Cell with an Inclined Carbon Block and a Copper Insert

Randhir Singh[1] · Kaushik Das[1] · Abhijeet K. Mishra[2] · Nabakishore Kalo[2]

Received: 18 July 2016 / Accepted: 14 October 2016 / Published online: 3 November 2016

Abstract Numerical models of a cathode block assembly in a Hall–Hèroult cell, comprising of liquid aluminium, carbon block, current collector, ramming paste and a copper insert were built and the finite element method simulations were carried out to model the cathode voltage drop (CVD), the current distribution and, the effect of geometrical parameters on the CVD. The objective of the study was to quantify the drop in the CVD for different cathode assembly design. Flat- and inclined-interface carbon block top-surface and a copper insert versus the conventional insert-free designs were simulated with a myriad of other geometrical parameters to optimise the design. The results informed about the optimum insert positioning to about 75 mm from the collector base and the energy saving possibilities due to reduction in the CVD with a cathode design with inclined-interface carbon block and copper insert in the collector bar.

Keywords Cathode lining · Aluminium reduction cell · Current collector · Copper insert · Cathode voltage drop

1 Introduction

Efficient Aluminium production has evolved tremendously since the invention of the Hall–Héroult process in 1886. The specific energy consumption (energy consumed in producing 1 kg of Al during electrolytic reduction) has dropped from ~60 kW/kg at the end of nineteenth century to 12.5 kW/kg in 2010 [1]. The quest for further improving the energy efficiency and the cost is still pursued very actively. A report by Choate and Green [2] for the US Department of Energy has projected the wet, drained cathode and the inert-anode technologies as the short term means having maximum impact in bringing down the energy cost in Al reduction. Long term Al reduction technologies of importance are *Carbothermic Al reduction* and *Kaolinite* (*$AlCl_3$, electrochemical*) *reduction*. One of the promising areas is to improve the cathode block design and assembly.

A cathode block is mainly made of carbon with a carbon steel insert at the bottom. The interface between the carbon block and the steel bar is sealed by pouring cast iron and letting it solidify. The cathode block exhibits about 0.3 V of voltage drop between the liquid aluminium top and the end of collector bar, henceforth termed the cathode voltage drop (CVD). Various material phases contribute to the CVD typically as in Table 1.

A design optimisation study by Blais et al. [4] suggested that the optimum design of the cathode corresponded to a geometry giving uniform current distribution at the surface of the cathode block. The optimum design had a wedge-shaped Cu insert at the bottom of the steel bar. The wedge shape spanned in horizontal as well as in vertical directions. The enhancement of cathode life from the improved cathode design was projected to be 20 % with a concomitant drop in CVD of 93 mV [4]. Das et al. [5] evaluated the performance of a steel collector bar vis a vis a Cu collector. A Cu collector bar having the same cross sectional area as a steel collector bar but 0.72 times the length of the steel bar, was predicted to have a saving of over 150 mV in the CVD as compared with the steel. Moreover,

✉ Randhir Singh
randhir@iitbbs.ac.in

[1] School of Minerals, Metallurgical and Materials Engineering, Indian Institute of Technology, Bhubaneswar, Orissa, India

[2] Tata International Limited, P S Srijan Tech Park, 13th Floor, DN 52, Sector V, Salt Lake City, Kolkata 700091, India

Table 1 The average contribution of various material phases towards the CVD [3]

Material phases	% Contribution to the CVD
Carbon	26
Carbon–metal interface	25
Inner metal (under carbon block)	18
Outer metal bar	31

a Cu collector bar offered a significant advantage over the similar sized steel collector bar with regard to the uniformity of current distribution over the entire cathode surface. Recently, Gupta et al. [6] studied the effect of modifications in an insert-free conventional collector bar onto the cell heat energy balance. Higher height to width ratio and higher electrical conductivity of the collector led to: (1) increased heat loss, (2) increase in horizontal current density in the metal pad and (3) lowering of the CVD. In another computational study, Gupta et al. [7] studied the impact of Cu insert inside the collector bar on the cell thermal balance and the CVD, keeping the cell insulation unchanged from the base case. All of the three insert models resulted in increased uniformity of the vertical current density with regard to the insert-free base case, with a concomitant drop in the CVD of 30–44 mV. However, the ledge thickness in the lower region increased detrimentally up under the anode shadow due to high heat loss via the collector. Thus, an improvement on the cell insulation would be warranted to contain the heat to stabilise the ledge and the steady cell operation.

An FEM study by Das et al. on the effect of CB inclination on the Lorentz field distribution revealed that a 5° inclination resulting in a flattened V shape of the CB layer in contact with the liquid Al could reduce the magnitude of the Lorentz force by 16–20 %. Feng et al. [8, 9] have evaluated novel stepped cathode designs. Industrial test on such a 168 kA cell were performed for one year by Chongqing Tiantai Aluminum Company in 2008. The new designs offered an advantage of current efficiency of 1.4 % over the conventional cell. Moreover, the energy requirement for the reduction dropped to 12,092 kWh/t-Al from 13,352 kWh/t-Al for the conventional cell—a significant saving in energy of 1260 kWh/t-Al! The improvement in the cell performance resulted from the enhanced stability of the cell, due to the suppression of the horizontal current in the liquid Al, and liquid aluminium circulation around the steps leading to higher Al_2O_3 dissolution and taming of the vertical amplitude of the waves. It was not clear, however, if the new cathode design made an economic sense after accounting for the fabrication and long-term durability aspects.

There were several studies [3, 6, 10, 11] including patents [12–15], showing the beneficial effect of novel cathode designs. The published literature very often dealt with a collector bar geometry that were difficult to fabricate. Moreover, there was room for further tailoring of cathode design. For example, the Cu-insert in the optimised design of the cathode in the study by Blais et al. [4] was a hard-to-fabricate into double-wedged structure. Such an insert would be hard to place in a traditionally rolled steel bar. Thus, an easy-to-fabricate cathode design need to be studied and optimised from practical stand point. One of the objectives of the present article is to evaluate the performance of a rod-like Cu insert in the CS collector bar with regard to the savings in the specific energy consumption due to reduction in the CVD. In addition, the effect of the change in the design of the cathode block assembly on other critical parameters such as the horizontal current density, uniformity of vertical current density etc. are also studied. For this purpose, a 3D *slice* model of the cell with novel composite (Cu-Steel) collector bar designs under a flat- or inclined-interface carbon block. The effect of various designs on the CVD and current distribution is investigated. The modelled cathode block assembly comprised of a metal pad, a carbon block and a collector bar with a Cu insert in some cases.

2 Model Description

A melting pot for the Al-reduction consists of a number of identical anodes. In this study, a reduction cell was considered as the equivalent portion of the pot under an anode. Due to inherent symmetry in the design of the melting pot, the present slice model concerned with half portion of such a cell—i.e., the equivalent area under half of an anode, consisting of:

1. Aluminium metal pad (Al)
2. Carbon block (CB)
3. Ramming paste (RP)
4. Carbon steel (CS), collector bar

Cathode assembly with an insert consisted, in addition, a Cu domain inside the CS. The cryolite bath layer and anode block were not modelled, as our primary interest is to model easily the CVD.

2.1 Model Geometry

The collector bar was modelled as just one piece or as a two piece bar with a copper insert placed wholly inside the CS bar. The insert free cathode assembly, termed as the *Base* models in this paper, had two variants: (1) flat surface CB and (2) inclined surface CB. Some of the dimensions in a flat CB surface cathode assembly, the Base-I model, are listed in Table 2. The thickness of an element was refered

Table 2 Dimensions of various material domains in the flat-surface CB model, i.e. the Base-I model

Parameter	Value (unit)
Width of the CB (w.CB)	500 (mm)
Width of the CS (w.CS)	77.5 (mm)
Thickness of the CB (t.CB)	480 (mm)
Thickness of the liquid Al (t.Liq.Al)	220 (mm)
Thickness of the CS (t.CS)	150 (mm)
Length of the CB (L.CB)	1880 (mm)
Length of the Al (L.Liq.Al)	L.CB
Length of the CS (L.CS)	2250 (mm)
Distance from the cell centre of CS (x0.CS)	100 (mm)
Thickness of the RP (t.RP)	50 (mm)

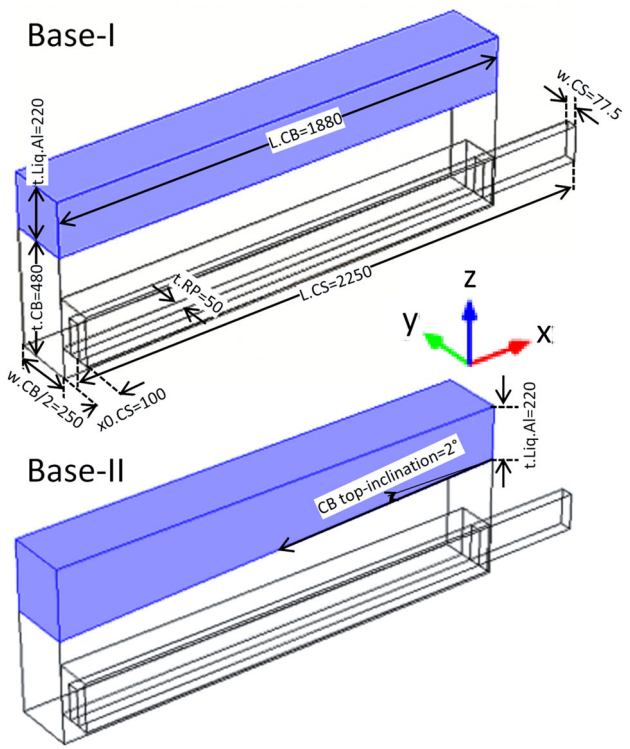

Fig. 1 Geometry of *Base-I* (flat CB surface) and *Base-II* (inclined CB surface, 2° to horizontal) models. The metal pool is highlighted in *light blue*. Dimensions are expressed in the unit of mm (colour figure online)

to as its dimension in vertical directions. The width and the length refered to the horizontal dimensions along the long channel and from centre to the outside of the cell respectively. The geometry of the *Base-I* and *Base-II* models are shown in Fig. 1.

In the Base-II model, the maximum thickness/height of the CB at the side-end was kept at 480 mm. The top surface of the CB had a downward slope of φ degrees (2° unless stated otherwise) with the horizontal direction,

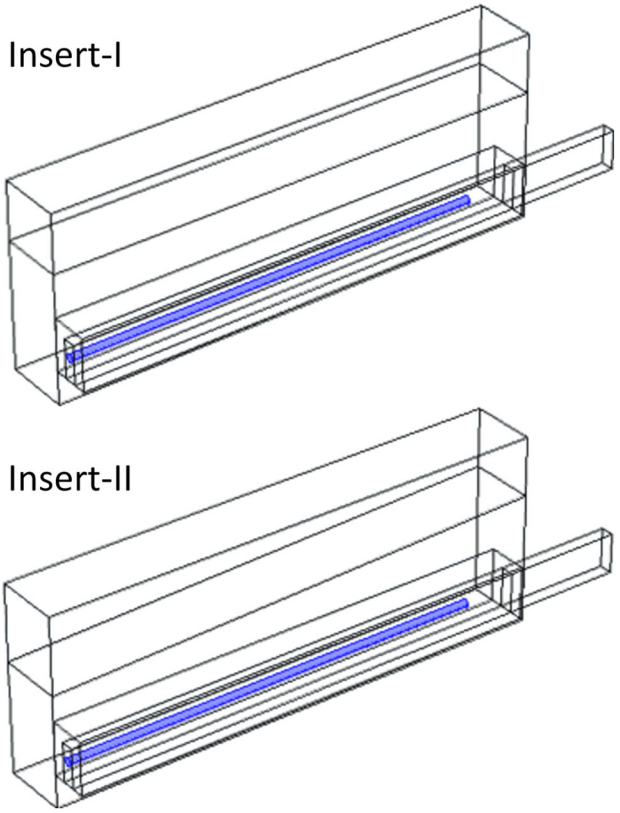

Fig. 2 Geometry of *Insert-I* (flat CB surface) and *Insert-II* (inclined CB surface, 2° to horizontal) models. The Cu insert is highlighted in *light blue* (colour figure online)

resulting in a deeper liquid Al pool at the centre of the cell. The liquid Al height at the outer end of the cell was fixed at 220 mm for all the models, including the *Insert* models.

Insert models had a copper insert with a uniform circular cross section. Two of its variants were studied:

1. Flat CB interface (*Insert-I model*) and,
2. Inclined CB interface (*Insert-II model*).

A parametric study was performed by varying the insert-related dimensions to (1) minimize the CVD and (2) to make the vertical current uniform with as little horizontal current component as possible. Typical Insert-I and Insert-II model geometry are shown in Fig. 2. The insert was always kept horizontal and, wholly inside the CS collector bar.

2.2 Model Physics

The computational model is essentially a coupled electro-thermal transport model, wherein the temperature and current distribution and the CVD in cathode block assembly were studied under a steady-state operation of the cell. Thermal model accounted for the effect of temperature on physical properties such as electrical conductivity, which

were supplied to the electrical model to compute the electric potential and other variables dependent on the potential. Electric model in turn provided the volumetric heat-source term due to the Joule heating to the thermal model. Thus, the only governing equation for the electrical balance was the constancy of the current density under the steady state condition, i.e.:

$$\nabla \cdot [-\sigma_x(T)\nabla\varphi] = 0 \tag{1}$$

where, $\sigma_x(T)$ is the temperature (T) dependent electrical conductivity in the material phase x, φ is the electric potential. Likewise, the only governing equation for the energy balance is:

$$\nabla \cdot [-k\nabla T] = \frac{1}{\sigma_x}\mathbf{J}.\mathbf{J} = \mathbf{J}.\mathbf{E} \tag{2}$$

where, k is the constant thermal conductivity and $\mathbf{E}$ the electric field. The current density vector, $\mathbf{J}$, could be calculated from the solution of the electric potential in Eq. (1) as:

$$\mathbf{J} = -\sigma_x(T)\nabla\varphi$$

The R.H.S. in Eq. (2) is the volumetric heat source due to the Joule heating.

The electrical conductivity of the CB, RP and CS varied with temperature as shown in Fig. 3. The electrical conductivity of the rest of the material domains were treated as constant.

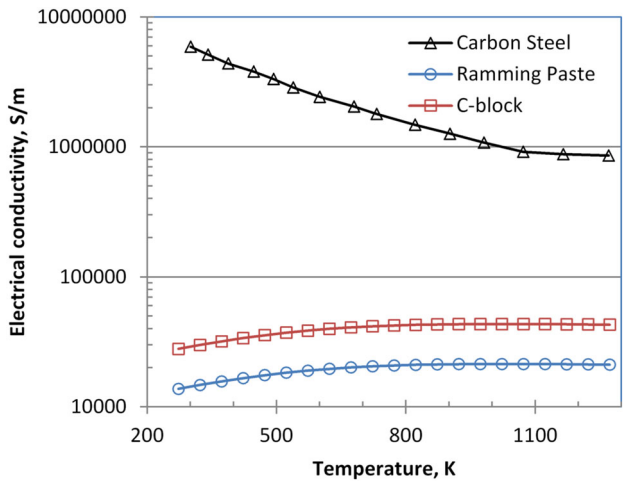

Fig. 3 Electrical conductivity of the CB, RP and CS as function of temperature

Table 3 Electrical contact resistance at the liquid Al–CB and the CS–RP interface

Parameter	Values	Explanation
Contact resistance at the CB–RP interface [16]	3.5×10^{-6} Ω m^2	Source is [16]
Contact resistance at the Al–CB interface	7.0×10^{-6} Ω m^2	A fitting parameter in the model

Electrical contact resistance at the CS–RP interface was taken from [16] (see Table 3). The value corresponded to a contact pressure of 0.5 MPa at the interface at 500 °C. Contact resistance at the Al–CB interface was a fitting parameter, determined by forcing the base-I model to yield the CVD value in a typical reduction cell of 272.1 mV. The procedure yielded a value of 7.0×10^{-6} Ω m^2 for the contact resistance at the Al–CB interface (see Table 3). There were no thermal contact resistance in the model.

Finally, all the coupled governing equations in the model were formulated for the steady state which required the specification of the boundary conditions as outlined below to make the problem well posed. It was noted, however, that the pot never operated under a constant voltage. Voltage fluctuations occurred due to metal-pad movement and a precise nature of such noises/fluctuations helped a great deal in operational process control and fault diagnosis [17, 18]. For purposes of modelling the cathode assembly, a steady state assumption during the cell operation made the problem tractable without compromising the accuracy.

2.3 Boundary Conditions and the Solution Methodology

The thermal (electrical) boundary conditions at the external boundaries were the same across all the models, shown in Fig. 4. A benchmark temperature of 573 K (maximum tolerable being 673 K) was often seen at the extremity of the collector bar [10]. Thus, the temperature at the extremity of the collector bar was set at 623 K. The bottom of the cell lining and the external surfaces including the collector bar surface were set at a temperature of 723 K. All the internal boundaries except the liquid Al–CB and RP–CS interfaces were modelled as perfect thermo-electrical contact across all models. The liquid Al–CB and RP–CS interfaces had perfect thermal contact but had a finite electrical contact resistance as is listed in Table 3. In the insert models, CS–Cu interface was modelled as a perfect contact. The aforesaid model was created, meshed and solved using finite element method (FEM) in a commercial software, COMSOL Multiphysics (COMSOL AB, Stockholm, Sweden). The mesh in the Base-I model had 95352 tetrahedral elements, generated with a built-in settings of "Physics-controlled + Extra fine" mesh (see Fig. 5).

3 Results and Discussion

The present study uses just one fitting parameter—the contact resistance at the Al–CB interface which is determined for once using the Base-I model. The electrical

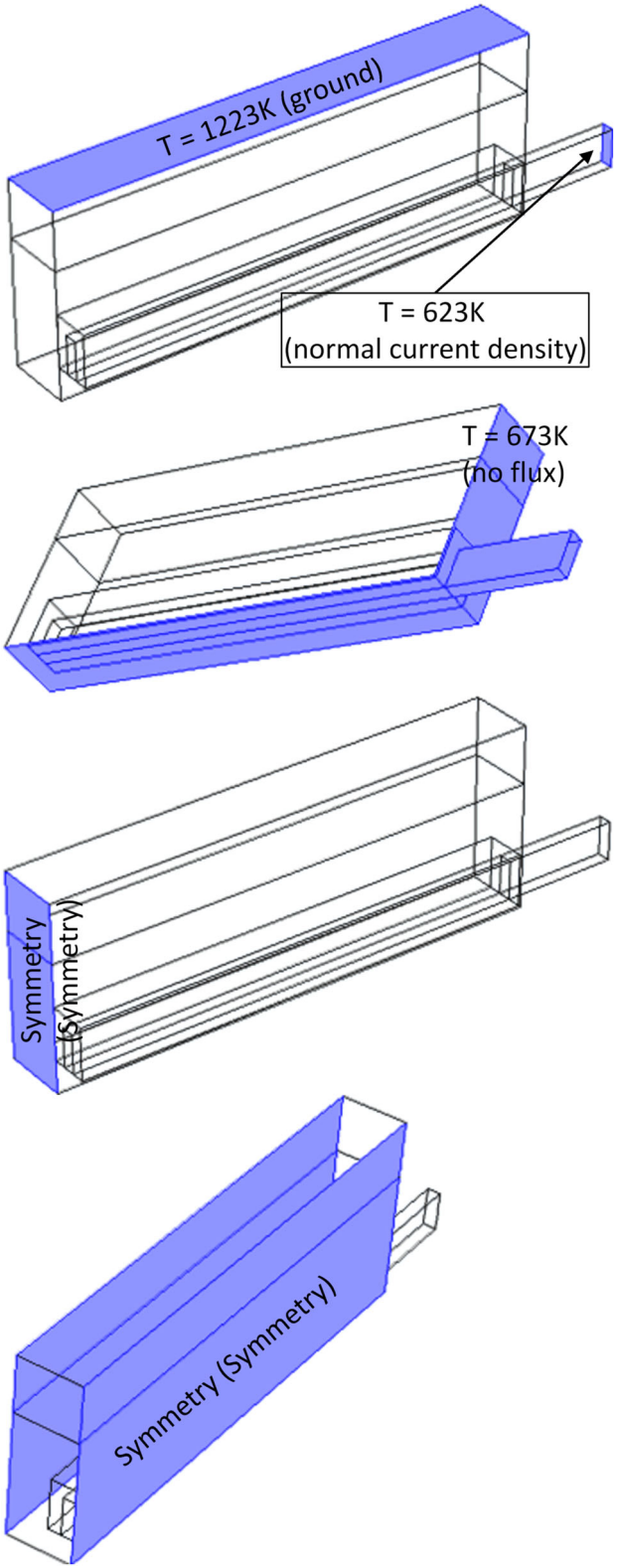

Fig. 4 Thermal (electrical) boundary conditions at the external boundaries, valid for all the models in this work

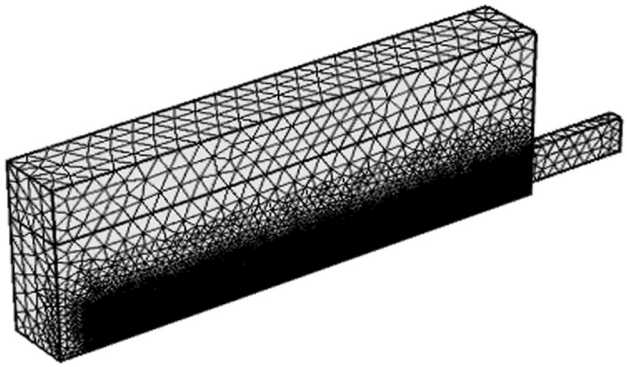

Fig. 5 A typical mesh generated with the built-in settings of "Physics-controlled + Extra fine" in COMSOL for the Base-I model

contact resistance at the Al–CB interface (see Table 3) has been numerically optimised to yield a CVD value in the Base-I case of 272.1 mV—a typical value observed in an operational cell. This value has been frozen once and for all for the purpose of development of the rest of the models. The contact resistance at the liquid Al–CB interface of 7.0×10^{-6} Ω m^2 is double that of the contact resistance at the CS–RP interface of 3.5×10^{-6} Ω m^2. This is due to the deposition of undissolved Al_2O_3 and other impurities at the former interface and, non-wettable characteristics of the carbon block. Also, an aluminium carbide surface layer, about 200 μm thick and in stratified condition, is formed at the carbon cathode during operation [19]. Due to its very small thickness, the carbide layer is not directly incorporated into our model. However, having low conductivity, the effect of this layer on the CVD can be modelled by a contact impedance at the liquid Al–CB interface.

In the following sections, the result of simulation on the Base-I/II and Insert-I/II models has been presented with regard to the total heat flux streamlines, the CVD and the uniformity of current distribution. In addition, parametric studies have been carried out in order to optimise the geometry.

3.1 Heat Flux Streamline

The total heat flux streamlines for four of the representative model cases is shown in Fig. 6. The average temperature in the CS—the material domain having strongest dependence of conductivity on temperature and carrying a huge current, for the Base-I, Base-II, Insert-I and Insert-II models are respectively 766.8, 768.6, 764.7 and 766.5 K (Table 4). The streamlines for the total heat flux in Fig. 6 demonstrate that most of the heat is being lost from the bottom of the cell or from the outer side of the cell. Rest of the cell surfaces (i.e. the face at the cell centre and the faces normal

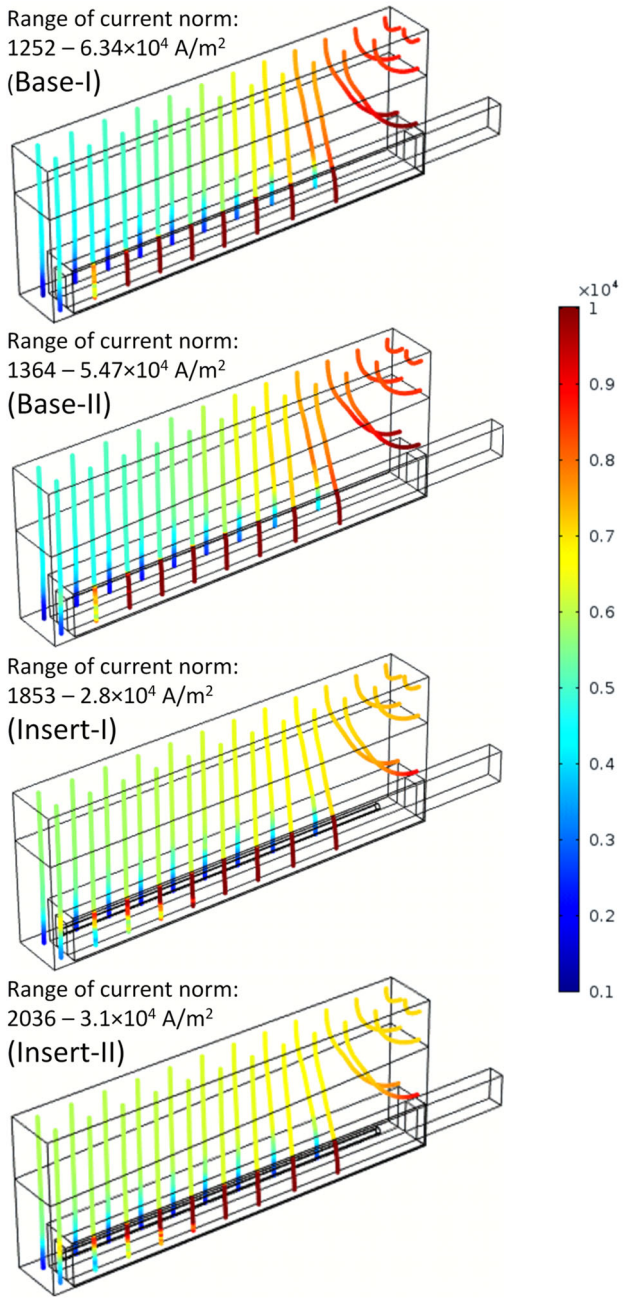

Fig. 6 Total heat flux streamlines for four of the representative model cases. Colour as per the current norm (colour figure online)

Table 4 CVD and the average temperature for the representative Base-I, Base-II, Insert-I and Insert-II models

Model identifier	CVD/ (mV)	Ave. temperature in the CS/(K)
Base-I (insert-free, flat surf. CB)	272.1	766.8
Base-II (insert-free, inclined CB)	268.4	768.4
Insert-I (Cylindrical insert; L.Cu = 1600 mm)	236.3	764.7
Insert-II (Insert-I with inclined CB)	231.8	766.5

to the longitudinal direction, *y*, of the pot) do not allow heat loss due to symmetric boundary condition. This is a good approximation for a cell near the middle of a pot. Not surprisingly, few studies [20–22] have modelled the heat losses from the pot via two parallel, one dimensional circuits—one towards the bottom of the cell and another towards the sides;—two directions with the highest temperature gradient. It is to be noted that over 50 % of the total heat loss from the cell is lost from the top of the cell [20]. Also, the colour scale of the thermal streamlines based on the current density norm demonstrates high current load towards the outer side of the cell. However, the range of the current density norm shrink in the order: Base-I, Base-II, Insert-II and Insert-I respectively, underscoring the beneficial effect of the insert as well as the inclination. It is to be noted that the outer side of the cell and the base of the cell have been modelled in such a way, as if they have a fixed temperature of 723 K. A better heat balance of the cell will result if an appropriate convective heat loss from the side of the cell and an accurate model of the cell lining is incorporated. In the present work, an approximate profile of the temperature captures the temperature dependent conductivities fairly well to simulate the CVD within tolerable limit.

3.2 Cathode Voltage Drop (CVD)

The CVD for the Base-I, Base-II, Insert-I and Insert-II models are listed in Table 4. The CB inclination and the Cu-insert both are effective in bringing down the CVD. The greatest impact obviously arises due to the Cu-insert of length 1600 mm, whereby the Insert-I model shows 36 mV lesser CVD as compared to the insert-free Base-I model. The same conclusion holds true for the inclined CB Insert-II model vis a vis the inclined CB insert-free model (Base-II). The implication of the CVD with respect to reduction of specific energy consumption is obvious: For example, a drop in CVD by 40 mV in a 200 kA cell, provides the cell stability and heat balance are taken care of and translates to a power saving of roughly 8 kW per melting pot. This kind of energy saving over the long run is projected not only to break even with the cost of design modification but also to generate a significant profit as well as lesser carbon footprint.

3.3 Uniformity of Current Distribution

Streamlines of the current density with a colour-scale as per the *x*-component of the current density are shown Fig. 7. The *x*-component of the current density is expected to be much dominant over the other horizontal component, i.e. the y component, as the current finally leaves the cell in the *x* direction and due to the cell symmetry there is no *y*-component of the current density at boundaries normal to *y*. The

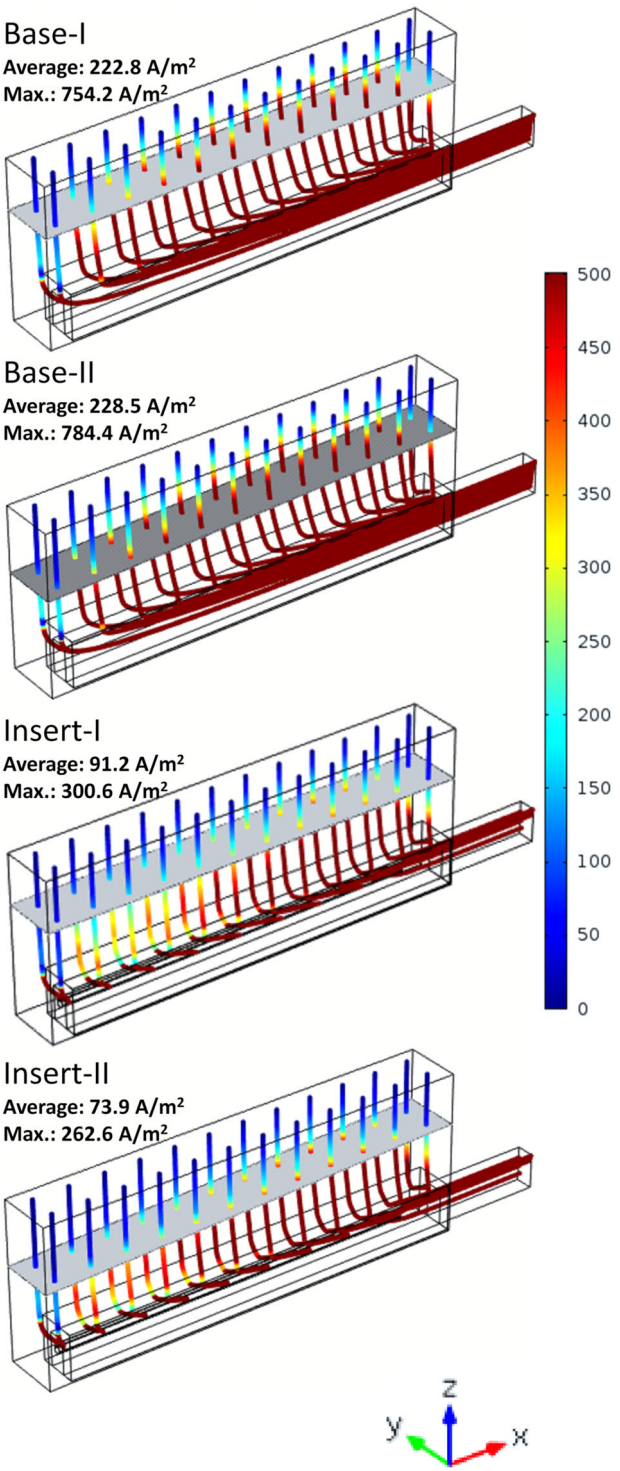

Fig. 7 Streamlines of the current density with a colour-scale as per the *x*-component of the current density (colour figure online)

horizontal (mainly *x*) component of the current density is known to interact with the z component of the magnetic flux density which is responsible for the notorious Magneto-Hydro-Dynamic (MHD) effect. The average and the maximum values of the *x*-component of the current density in the

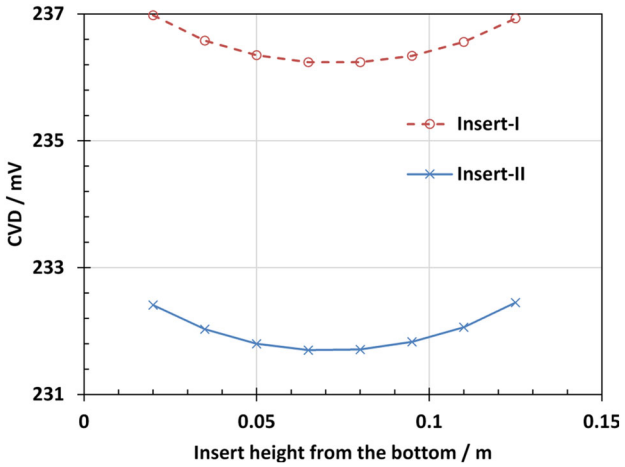

Fig. 8 Effect of the insert height from the bottom of the cathode assembly

liquid Aluminium pool is also noted. The average value of the *x*-component of the current density are 223 (Base-I), 229 (Base-II), 91 (Insert-I) and 74 (Insert-II) A/m^2 respectively. To rationalise this trend we need to understand the effects of (1) a CB inclination and (2) a Cu insert, on vertical and horizontal resistances to current flow. An inclination of the CB results in reducing the vertical resistance by replacing the low conducting CB by the liquid Al progressively towards the centre of the cell and reduces the vertical to horizontal resistance ratio. A lower resistance ratio leads to the increase in the maximum total current density [10]. The horizontal, *x*-component of the current density also follows the same pattern as for the total current density. Thus, the marginal increase in the average and the maximum values of the *x*-component of the current density in Base-II from the respective values in Base-I can be attributed to a reduction in the vertical to horizontal resistance ratio.

Similarly, an insert in the collector bar lowers the horizontal resistance and thus, increases the ratio of the vertical to horizontal resistance. The increase in the ratio evens the total current distribution [10]. Therefore, the average and the maximum values of the *x*-component of the current density in Insert-I is less than half the respective values in Base-I. Finally, in the Insert-II case, the ratio of the vertical to horizontal resistance to current flow will be lower than in the Insert-I case due to the increase in the depth of the liquid pool at the expense of the low conducting CB. The increase in this ratio leads to a higher maximum values of the *x*-component of the current density; however, the average values of the *x*-component of the current density decreases as compared with the Insert-I case. Therefore, it is suspected that a Cu insert inside the CS along with an inclined CB are producing some synergistic effect in lowering the average values of the *x*-component of the current density.

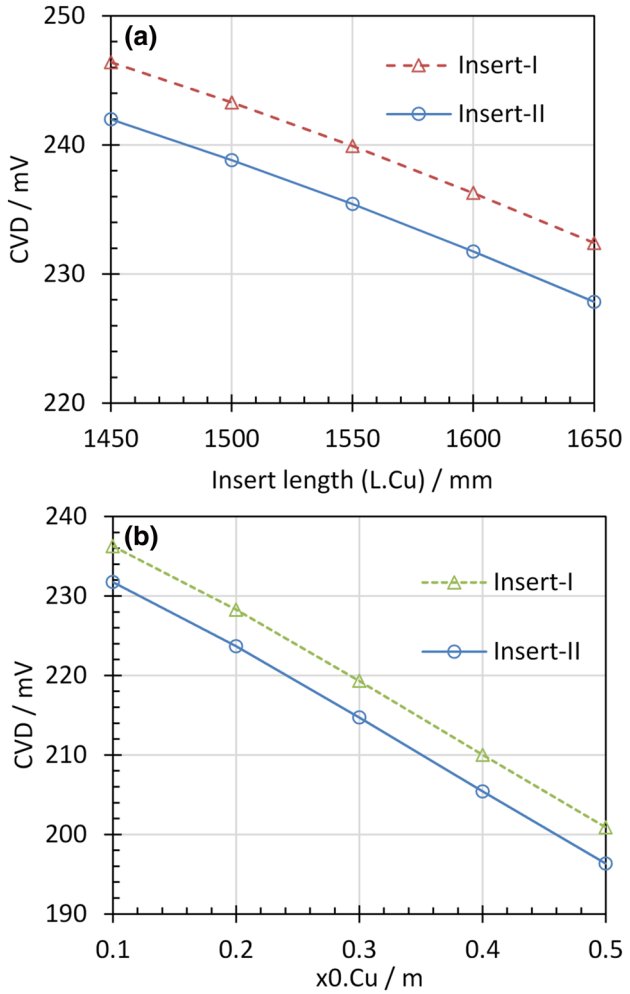

Fig. 9 Effect of **a** length and **b** placement (distance from the centre of the cell, x0.Cu) of the Cu-insert on CVD

3.4 Parametric Studies

The following parameters have been systematically varied to study their effect on the CVD in the insert models:

1. Height of horizontal Cu-insert (h.Cu)
2. Length and placement (distance from the centre of the cell) of the Cu-insert
3. CB inclination

The CVD initially drops with an increase in the vertical height of the horizontal Cu-insert upto a value for h.Cu equaling 75 mm. It then increases again with the height forming an inverted bell shape (see Fig. 8). The height varies from a minimum of 20 to 150 mm. Thus, an optimal value for the h.Cu will be about 75 mm. However, its advantage over CVD is really small ($\approx$1 mV maximum). The inverted bell shape can arise due to the change in the electrical conductivity brought about by a change in the temperature profile, despite the fact that the vertical

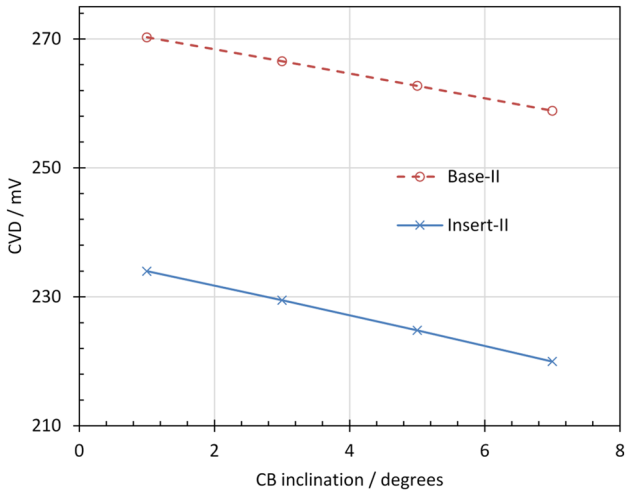

Fig. 10 Drop in CVD with an increase in the inclination of the top surface of the CB

resistance to current flow will be lower, as the value of h.Cu is higher.

The length and placement (distance from the centre of the cell, x0.Cu) of the Cu-insert also influences the CVD. As is clear from Fig. 9, the drop in CVD with length and with x0.Cu has been found to be linear in both the Insert-I and Insert-II cases. The drop in CVD with the insert length and with x0.Cu has been found to be 0.7 and 0.9 mV/cm respectively for both of the Insert models.

Lastly, the drop in CVD with an increase in the inclination of the top surface of the CB has been found to be linear (see Fig. 10). Magnitude of the CVD drop has been found to be 1.9 and 2.3 mV/° of CB inclination for Base-II and Insert-II models respectively. The drop in CVD is due to the reduction in overall resistance to current flow.

3.5 Optimizing the Insert Amount

Having quantified the drop in CVD with varius geometrical parameters of the cathode assembly design, a question arises as to what is the optimum Cu insert material to be used? The answer to the question is dependent on our objective function. If we choose the drop in CVD as our objective function with the constraints of a cylindrical rod-like insert geometry wholly inside the collector bar, the optimised length of the insert spans the whole length of the collector bar with its diameter equal to the collector bar width. That is to say that the optimum Cu usage for the minimum CVD corresponds to the maximum copper amount under the imposed constraints. However, not all material fractions of the insert have been equally efficient in bringing down the CVD. Farther the portion of the insert towards the outer extremity of the collector bar, more efficient it becomes in bringing down the CVD. This

follows from the fact that the outer end of the collector/insert bar carries more current than its interior counterpart.

On the ground, what trumps as the ultimate objective function is not the minimum of CVD but it's the saving over the full operational period of the cell. Such an objective function is a net sum of many factors such as, the savings due to: (1) less energy consumption, (2) longer cell-lining life, (3) lower carbon block erosion and (4) reduction in anode to cathode distance; and the cost associated with the (1) copper material, and (2) the material fabrication. Attaching a reasonable values to the above components of the objective function is a non-trivial exercise and, outside the scope of the present work. However, some optimisation works using a preliminary version of the aforesaid objective function is presented in [4] and [10].

4 Conclusions

A numerical model of the cathode block assembly in a Hall–Heroult cell was built and the finite element method (FEM) simulations were carried out to model mainly the cathode voltage drop (CVD) and the current distribution in a conventional insert-free cathode assembly (Base models) as well as in an assembly with a horizontal copper insert, wholly inside the CS (Insert models). The typical CVDs for the four representative models were found to range from 231.8 to 272.1 mV (see Table 4).

It was clear that a voltage reduction of $\sim$40 mV over and above the Base-I case, i.e. a conventional cathode assembly, seemed well within reach by using a copper insert. The Insert-I and Insert-II models showed a further reduction of about 20 mV if we could place the copper rod toward the exterior of the collector bar, utilising the same quantity of Cu.

Insert group models demonstrated that the magnitude of the average as well as the maximum values of the horizontal component of the current density in the liquid metal pool was more than halved as compared to the respective values for the Base group models. Geometrical optimisation suggested the placing of the Cu-insert at 75 mm from the base of the assembly for the maximum saving in the CVD. For a fixed length Cu-insert, placing it to the end-side (outer end) of the collector bar resulted in the maximum drop in CVD. A *linear* drop in CVD was found with the increment of the following parameter:

1. Insert length (0.7 mV/cm for both of the Insert model)
2. Insert distance from the centre of the cell (0.9 mV/cm for both of the Insert model)
3. Inclination of the top surface of the CB (1.9 mV/deg. for the Base-II and 2.3 mV/deg. for the Insert-II)

Finally, the optimum insert material required to optimise the CVD to its' minimum, corresponded to the maximum allowed by the geometrical constraints of a cylindrical shape, horizontal alignment and placement inside the steel collector bar. It is suggested that the total cost saving over the cell life be optimised rather than working on a cell performance metric such as the CVD.

References

1. R. von Kaenel and J. Antille, *Light Met. 2011*.
2. W. T. Choate and J. A. S. Green, "US energy requirements for aluminum production: historical perspective, theoretical limits and new opportunities," US Department of Energy, Energy Efficiency and Renewable Energy, BOOK, 2003.
3. R. Beeler, "An analytical model for cathode voltage drop in aluminum reduction cells," in *LIGHT METALS-WARRENDALE-PROCEEDINGS-*, 2003.
4. M. Blais, M. Désilets, and M. Lacroix, *Appl. Therm. Eng.*, vol. 58, 2013.
5. S. Das, Y. Morsi, and G. Brooks, *JOM*, vol. 66, 2014.
6. A. Gupta, S. Modak, M. Sahoo, and J. Janardhanan, in *Light Metals 2015*, John Wiley & Sons, Inc., 2015.
7. A. Gupta, A. Jha, M. Sahoo, J. Jinil, and J. P. Nayak, in *The International Committee for Study of Bauxite, Alumina & Aluminium*, 2015.
8. F. Naixiang, T. Yingfu, P. Jianping, W. Yaowu, Q. Xiquan, and T. Ganfeng, *Essent. Readings Light Met. Alum. Reduct. Technol. Vol. 2*.
9. Y. Song, J. P. Peng, Y. W. Wang, Y. Z. Di, B. K. Li, and N. X. Feng, *Metalurgija*, vol. 55, 2016.
10. M. Gagnon, P. Goulet, R. Beeler, D. Ziegler, and M. Fafard, *Light Met. 2013*.
11. R. von Kaenel, J. Antille, and L. Bugnion, in *Light Metals 2015*, John Wiley & Sons, Inc., 2015, pp. 807–812.
12. P. Morel, "Construction of the lower part of the crucible of igneous electrolysis cells," US 2846388 A, 05-Aug-1958.
13. B. Allano, D. Bonnafous, J. Camire, M. Desilets, L. Fiot, P. Fournier, Y. Gauthier, D. Laroche, O. Martin, and P. Thibeault, "Electrolysis cell for the production of aluminum comprising means to reduce the voltage drop," EP1927679 A1, 06-Aug-2013.
14. E. Hagen and B. ØYE, "An electrode for aluminium production and a method of making same," WO2014116117 A1, 31-Jul-2014.
15. K. R. Von and G. Spinetti, "Cathode current collector for a Hall–Heroult cell," WO2016079605 A1, 26-May-2016.
16. L. St-Georges, L. Kiss, and D. Marceau, *Minerals, Metals and Materials Society/AIME, 420 Commonwealth Dr., P. O. Box 430 Warrendale PA 15086 USA.[np]. 14-18 Feb*. Minerals, Metals and Materials Society/AIME, 420 Commonwealth Dr., P. O. Box 430 Warrendale PA 15086 USA, 2010.
17. A. Agnihotri, S. U. Pathak, and J. Mukhopadhyay, *Trans. Indian Inst. Met.*, vol. 67, 2014.
18. A. Agnihotri, S. U. Pathak, and J. Mukhopadhyay, *Trans. Indian Inst. Met.*, vol. 67, 2014.
19. Ø. Østrem, "Cathode wear in Hall–Héroult cells," JOUR, Norges teknisk-naturvitenskapelige universitet, Fakultet for naturvitenskap og teknologi, Institutt for materialteknologi, 2013.
20. M. P. Taylor, W. D. Zhang, V. Wills, and S. Schmid, *Chem. Eng. Res. Des.*, vol. 74, 1996.

21. V. Gusberti, D. S. Severo, B. J. Welch, and M. Skyllas-Kazacos, *Light Met.*, vol. 2012, 2012.
22. V. Gusberti, D. S. Severo, B. J. Welch, and M. Skyllas-Kazacos, "Modelling the Aluminium Smelting Cell Mass and Energy Balance–a Tool Based on the 1st Law of Thermodynamics," in *Proceedings of 10th Australian Aluminium Smelting Technology Conference, Launceston, TAS*, 2011.